Journal of Materials and Engineering Structures

Research Paper

Numerical simulation and reliability of behaviour until the rupture of reinforced concrete spacial structure members with circular cross section

Djamal Bouchafa [a], Mohand Said Kachi [a,], Youcef Bouafia [a], Karim Benyahi [a], Salma Barboura [b]*

[a] *LaMoMs Laboratory, University Mouloud Mammeri of Tizi-Ouzou, 15000 Tizi-Ouzou, Algeria.*

[b] *C.N.R.S. LSPM – UPR 3407 Laboratory, Paris 13 university, Paris, France.*

ARTICLE INFO

Article history:

Received : 2 October 2020

Revised : 27 January 2021

Accepted : 29 January 2021

Keywords:

Numerical simulation

Circular cross section

Reliability

Reinforced concrete

Monte Carlo method

ABSTRACT

Numerical simulation of simple and composed bending behaviour of reinforced concrete spatial structure elements with circular cross section in the field of nonlinear elasticity, require a particular modeling's technique of the cross section shape by a subdivision of the latter into trapezoids to best approximate the contour of the cross section. The input and output parameters of the materials behaviour modeling are simulated by random and deterministic variables. The present study aims at proposing a technique of the behaviour's simulation up to failure taking into account the material non-linearity on the reinforced concrete structural elements with a circular cross section; a comparison was made between our simulation results and the experimental results. On the other hand, a numerical method has been modeled which makes it possible to estimate the reliability and the probability of failure of our simulation. To validate this modeling, we performed another comparison of the results obtained from our mechanical model by a Monte Carlo simulation with a reliable Hasofer-Lind method

1 Introduction

Most of the research carried out on the non-linear calculation of reinforced concrete structures is concentrated on rectangular sections, however, reinforced concrete structures with solid circular cross section are habitually used in civil engineering construction, for example as pile foundations, columns of reinforced concrete buildings, etc. The material nonlinear analysis has been established first in order to obtain the real behaviour of materials by using two main methods widely used to characterize the real behaviour of reinforced concrete structures. The first method is known as "incremental method", the second one is called "the initial deformation method". In addition to the material nonlinear analysis, the geometric nonlinear analysis has been also used in the aim of characterizing the real behaviour of structures. Yagmai [1] has

* *Corresponding author. Tel.: +213 552312836*
E-mail address: kachi_ms@yahoo.fr

e-ISSN: 2170-127X,

RESEARCH REVIEW of Sciences and Technologies

updated the Lagrangian description to establish the general formulation of geometric nonlinear analysis. These two nonlinearity analyses approaches have been jointly used for the first time by Grelat [2], Sargin [3] has modelled the compressed concrete law behaviour, the tensed zones were simulated using a behaviour law where the concrete is represented by a triangular fictitious stress diagram from the neutral fiber. Naït-Rabah [4] and Iguetoulene and al [5]. has extended the numerical simulations to three-dimensional structures. Considering large displacements and rotations, Robert [6] has introduced co-rotational motion for the treatment of geometric nonlinearity. an analytical model for modelling reinforced concrete structures in nonlinear elasticity has been proposed by [7-9]. In these classical studies about this subject, shear strength is neglected or taken into account by simple formulæ of the theory of linear elasticity. In the case of the structure's shear behavior, Kachi and al [10] and Vecchio and al [11] are introduced the notion of the variable shear modulus, on the reinforced and prestressed concrete structures calculation, with the shear variation.

Hanover, in general, the calculation of reinforced concrete structures with regular sections is a well-known problem. In the particular case of circular sections or annular sections, analyzing the behavior of the section has been subject to the several studies we can mention [12-14].

Probabilistic methods can be distinguished in: random methods, as Monte Carlo Simulations, Importance Sampling, etc., have been largely used to estimate the failure probability of structures. And non-random methods which consist on estimating the Failure Surface (FS), called also: limit state. The Response Surface Method (RSM) is particularly recommended to analyze reliability of nonlinear structures with implicit FS. So far, few studies on reinforced concrete structures using reliability analysis have been published. Here, we took some examples where this topic is studied, the reliability of reinforced concrete columns and bridges appear in the work realized by Frangopol and al. [15], wherein the load correlation and the load program can affect the reliability. Reid [16] has also studied the reliability problem in reinforced concrete columns, but focusing the long-term effects and the loss of strength due to the duration of loading. Other authors have also studied reinforced concrete columns such as, for example, Holicky & Vrouwenvelder [17] who studied the reliability index in term of time. His work was conducted by applying long and short-term actions, for which the reinforced concrete element behaviour was represented by a bending moment-normal force relationship, applying the FORM method to approximate the failure integration. Val and al. [18] presented a technique built on a combination of a finite element model with FORM method, applied to estimate the probability of failure of the nonlinear reinforced concrete frame taking into account the geometric and physical non-linearities. Benyahi and al. [19] has developed a model to estimate the reliability of metallic structures.

In this paper, the required response is achieved by means of the displacement method which considers non-linear behaviour through beams theory. The method presented take account the nonlinear materials behavior and it consider a variable shear modulus as function of the shear variation. The three-dimensional finite element discretization of the beam structure take the shape of straight sections decomposed into trapezoids. This method allows us to describe the real behaviour until the rupture of the structures. The reliability design is constructed by coupling a non-linear finite element model with the RSM method, and structural safety is provided through the Hasofer-Lind reliability index, which is obtained by solving the optimization problem, for which the Rackwitz and Fiessler algorithm has been used. In this work, we established a program in Fortran to simulate the Direct Monte Carlo method coupled with a non-linear calculation to assess the probability of failure of reinforced concrete spatial structure elements with a circular cross section.

The paper is structured as follows: in the first part, we provide the different laws of the material's behaviour, then we present the calculation's method of the mechanical model, after that; we describe the section's equilibrium and the global beams element's equilibrium. In the second part, we present two probabilistic methods to evaluate the reliability of the examples studied in the context of nonlinear analysis. Lastly, we check the validity of our mechanical model by comparing our numerical results with experimental results, then; we verify the results of the reliability model; and this by comparing the results achieved by direct Monte-Carlo simulation with those of the Hasofer-Lind method.

2 Constitutive models of materials

2.1 Compression Behaviour of the Concrete

Different mathematical models of concrete are presently used in the analysis of reinforced concrete structures. In this study, the monotonic curve presented by Sargin [3] was adopted for its simplicity and computational efficiency (see Fig. 1).

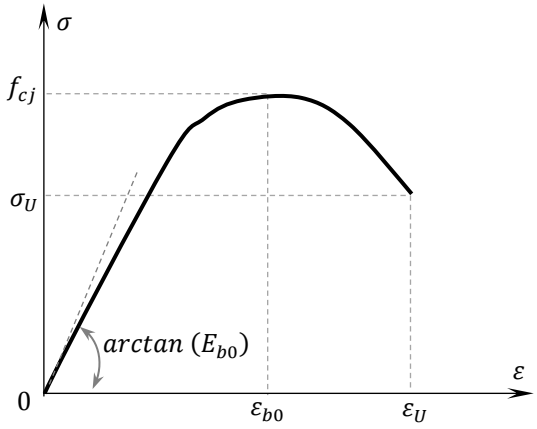

Fig. 1 – Behaviour of ordinary concrete in compression Sargin [3].

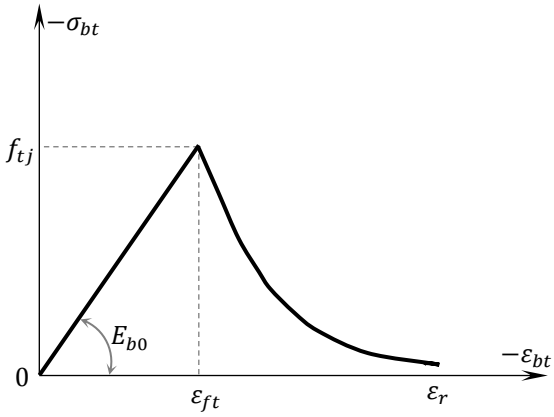

Fig. 2 – Stress-strain behaviour of ordinary concrete Grelat [2]

In this model, the stress is linked to the strain by eq. (1):

$$\sigma = f_{cj}\frac{k_b\cdot\bar{\varepsilon}+(k_b'-1)\cdot\bar{\varepsilon}^2}{1+(k_b-2)\cdot\bar{\varepsilon}+k_b'\cdot\bar{\varepsilon}^{2\prime}} \tag{1}$$

where $\bar{\varepsilon}=\dfrac{\varepsilon}{\varepsilon_{b0}}$ and $E_{b0}=11000\cdot\sqrt[3]{f_{cj}}$

For a normal concrete, it usually takes by : $k_b'=k_b-1$, k_b is given by the following equation: $k_b=\dfrac{E_{b0}\cdot\varepsilon_{b0}}{f_{cj}}$.

2.2 Tensile Behaviour of Concrete

We assume that the concrete behaviour is linearly elastic in the tension region. After the concrete cracking strain, the tensile stress decrease with increasing the tensile strain. In this field, we have adopted the monotonic concrete stress-strain curve introduced by Grelat [2] for describe this decreasing branch (see Fig. 2). Ultimate failure is assumed to take place by cracking when the tensile strains exceed the yielding strain of the reinforcement. In this model, monotonic concrete tensile behaviour is described by Eq. (2).

$$\begin{cases}\sigma_{bt}=E_{b0}\cdot\varepsilon_{bt} & if\ \ |\varepsilon_{bt}|\le\varepsilon_{ft}\\ \sigma_{bt}=-f_{tj}\dfrac{(\varepsilon_{bt}-\varepsilon_{rt})^2}{(\varepsilon_{rt}-\varepsilon_{ft})^2} & if\ \ \varepsilon_{ft}<|\varepsilon_{bt}|\le\varepsilon_{rt}\\ \sigma_{bt}=0 & if\ \ |\varepsilon_{bt}|>\varepsilon_{rt}\end{cases} \tag{2}$$

2.3 Reinforcement Constitutive Law

Reinforcing steel is modelled as perfect elastoplastic law**.** Extreme strains are defined by BAEL [20] as 10 ‰.

$$\begin{cases}\sigma=E_a\cdot\varepsilon & if\ \ 0\le\varepsilon_r<\varepsilon_e\\ \sigma=\sigma_e & if\ \ \varepsilon_e\le\varepsilon\le\varepsilon_u\\ \sigma=0 & if\ \ \varepsilon>\varepsilon_u\end{cases} \tag{3}$$

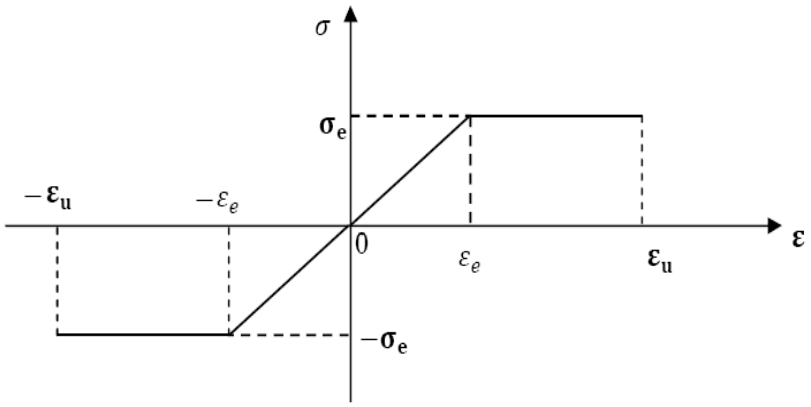

Fig. 3 – Stress-strain diagram of a natural steel (Perfect elastoplastic law) BAEL [20]

2.4 Concrete Shear Modulus:

In this present study, the formulas proposed by Adjrad and al. [21] for calculating the shear modulus of concrete is adopted. The shear modulus is calculated in the three phases of the behaviour.

Phase 1: Before concrete cracking, the theory of linear elasticity is valid, the transverse deformation modulus Gis a function of the longitudinal deformation modulus E_c of the concrete at the origin, and it is given by Eq. (4).

$$G = \frac{E_c}{2(1-\mu)} \quad \text{for} \quad 0 \le \gamma \le \gamma_{fiss} \tag{4}$$

Phase 2: After concrete cracking and before steel yielding, the transverse deformation modulus Gis a function of concrete's and steel's characteristics; see Eq. (5).

$$G = 604\,w \quad \text{for} \quad \gamma_{fiss} \le \gamma \le \gamma_{plas} \tag{5}$$

Phase 3: This phase corresponds to the steel yielding; the transverse deformation modulus G is a function of the materials' characteristics see Eq. (6).

$$G = 327\,w \quad \text{for} \quad \gamma_{plas} \le \gamma \le \gamma_{fr} \tag{6}$$

where: $\gamma_{fiss} = 0.0003$; $\gamma_{plas} = 0.0025$; $\gamma_{fr} = 0.006$; $\mu = 0.2$; and we note: $w = \dfrac{\rho_t\ f_{et}\ \rho_l\ f_{el}}{f_{cj}}$

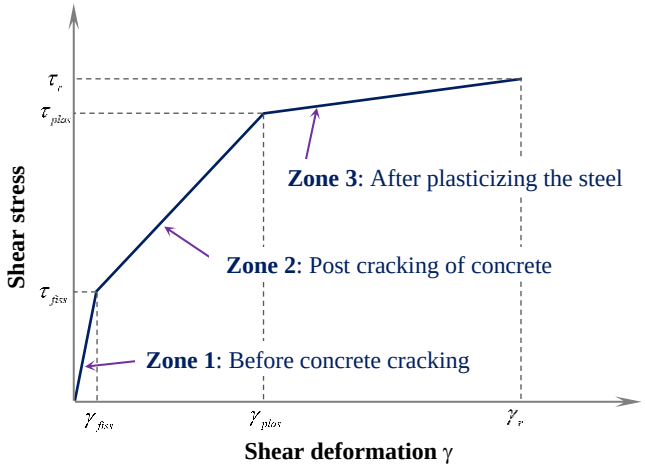

Fig. 4 – Schematic presentation of the overall behaviour Shear stress-strain Adjrad and al. [21]

3 Procedure for calculating the equilibrium state of the element

In what follows, we will admit:

The assumption of small deformations, the assumption of small displacements, the assumption of flat sections, the principle of superposition of effects, the assumption of a perfect adhesion between the reinforcement and the section and the materials follow laws of uniaxial behaviour.

3.1 Coordinate system

In the global axis system $x_G y_G z_G$, one positions of the local axis system $X_0 Y_0 Z_0$ of the element associated with here initial position, at the increasing of the loading, I_0 and J_0 nodes of the element are moved in I and J, respectively, and then introduced the concept of intrinsic axis system, noted XYZ.

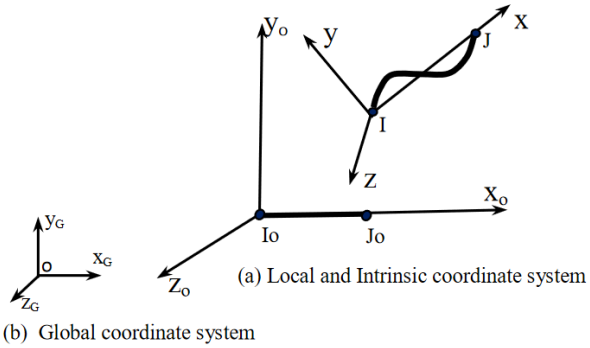

Fig. 5 – Axis system of an element in 3D initial and deformed state of the element

3.2 Equilibrium of the section

The normal deformation of a section is written as $\varepsilon_x(y) = \varepsilon_g + z.\phi_y + y.\phi_z$ and its transverse deformation is defined by γ_y, γ_z and ϕ_z. The impact of this deformation is taken into consideration by a nonlinear approach.

The deformation increase vector of the section is given by Eq. (7):

$$\{\Delta\delta\} = \left(\Delta\varepsilon_g, \Delta\phi_y, \Delta\phi_z, \Delta y_y, \Delta y_z, \Delta\phi_x\right)^T \tag{7}$$

The section of concrete was considered as a succession of trapeziums. Each trapezium was defined by the dimensions of its lower and upper base $\left(b_j, b_{j+1}\right)$ and their ordinates $\left(y_j, y_{j+1}\right)$, relative to the reference axis passing through the section's center of gravity (see Fig. 6).

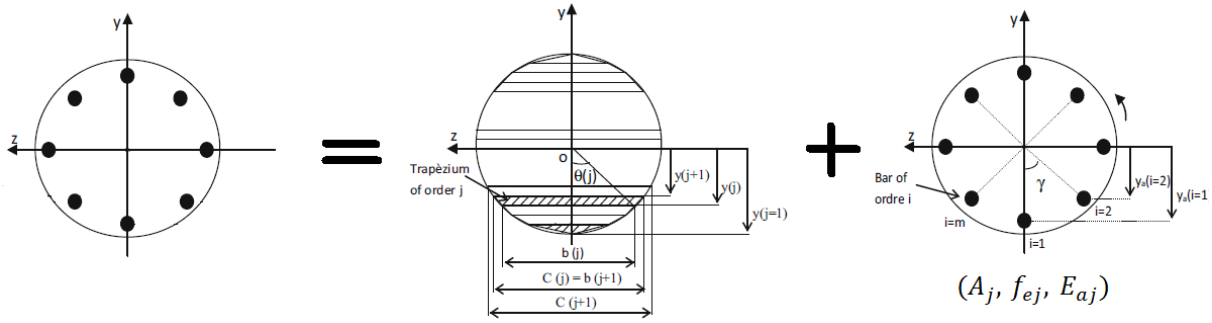

Fig. 6 – Section of beam with circular cross-section discretized in layers

The integration process is numerical, it is indispensable to express the widths and the ordinates of the trapeziums consistent with the numerical calculation relations.

$$B(y) = b_j + \left(b_{j+1} - b_j\right)\left(y - y_j\right) / \left(y_{j+1} - y_j\right) \tag{8}$$

The section of each longitudinal reinforcement is concentrated in its gravity centre. The cross-section of each right transverse reinforcement is assumed to be constant over the entire height of the section and distributed over the entire length of the section. The passive reinforcements are therefore defined as a succession of frames beds. Each bed is defined by its ordinate y_{ai} and by the total area of the longitudinal and transverse reinforcement located at this level A_j.

The equilibrium equation of the section in the intrinsic axis system can be written as Eq. (9):

$$\{\Delta F_s\} = [K_S]\{\Delta\delta\} \tag{9}$$

where

$$\{\Delta F_s\} = \left(\Delta N(x), \Delta M_y(x), \Delta M_z(x), \Delta V_y(x), \Delta V_z(x), \Delta M_c(x)\right)^T \tag{10}$$

Equation (9) is solved by means of an iterative method. Its solution can be given as Eq. (11):

$$\{\Delta\delta\} = [K_S]^{-1}\{\Delta F_s\} \tag{11}$$

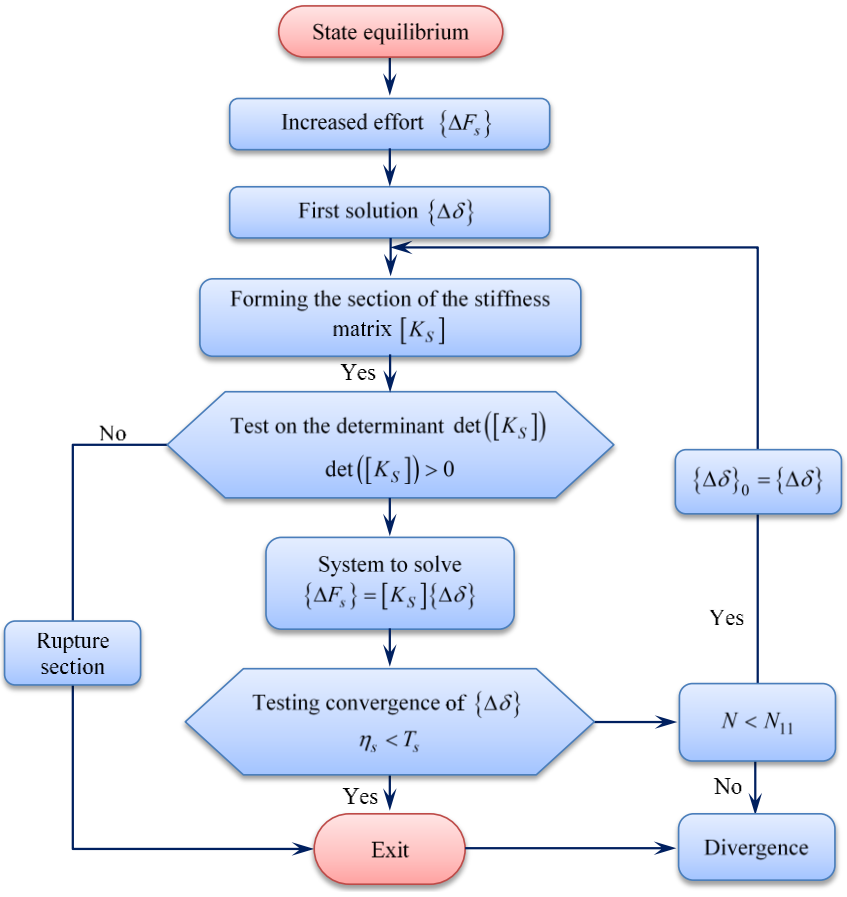

Fig. 7 – Flowchart of the research of the equilibrium of a section

3.3 Stiffness matrix of the element in the intrinsic axis system

Loads applying over the section are functions of the applied forces at the element nodes. Their expression is written as Eq. (12):

$$\{\Delta F_s\} = \left[L(x)\right]\{\Delta F_n\} \tag{12}$$

where $\left[L(x)\right]$ is the matrix connecting the loads acting on the section and the forces applied to the nodes of the element, it is given by:

$$\left[L(X)\right] = \begin{bmatrix} -1 & 0 & 0 & 0 & 0 & 0 \\ 0 & (1-X/L) & 0 & 0 & -X/L & 0 \\ 0 & 0 & -(1-X/L) & 0 & 0 & X/L \\ 0 & 0 & 0 & 0 & 0 & 1/L \\ 0 & -1/L & 0 & 0 & -1/L & 0 \\ 0 & Y_c/L & Z_c/L & -1 & Y_c/L & Z_c/L \end{bmatrix}$$

where X the abscissa of the cross section relative to intrinsic axis system, and L the length of the element after deformation.

If the length variation of the element is neglected, the expression of the deformation vector $\{\Delta S_n\}$ of the beam element, in the intrinsic axis system, is given by means of the virtual work theorem which stipulates that the virtual work of the section's deformations increase is equal to the virtual work of the section's loads increase, see relation (13):

$$\{\Delta S_n\} = \int_0^L \left[L(x)\right]^T \{\Delta\delta(x)\}\, dx \tag{13}$$

In consequence, we can write the equilibrium equation of the element in the intrinsic axis system as eq. (14):

$$\{\Delta F_n\} = [K_n]\{\Delta S_n\} \tag{14}$$

The stiffness matrix $[K_n]$ of the element evaluated as follows:

$$[K_n]^{-1} = \int_0^L \left[L(x)\right]^T [K_S]^{-1} \left[L(x)\right] dx \tag{15}$$

3.4 Global Equilibrium of the beam's element

The second order effects are introduced by transforming the equation from intrinsic axis system to intermediate axis system. In fact, the relationship between the expressions of the displacement in intrinsic and intermediate axis systems, using a geometrical transformation matrix $[B]$, may be given as Eq. (16):

$$\{\Delta S_n\} = [B]\{\Delta S_u\} \tag{16}$$

with

$$[B]=\begin{bmatrix} 1 & v/L_0 & w/L_0 & 0 & 0 & 0 & 0 & 0 & 0 \\ -w/L_0^2 & 0 & 1/L_0 & 0 & 1 & 0 & 0 & 0 & 0 \\ v/L_0^2 & -1/L_0 & 0 & 0 & 0 & 1 & 0 & 0 & 0 \\ 0 & 0 & 0 & -1 & 0 & 0 & 1 & 0 & 0 \\ -w/L_0^2 & 0 & 1/L_0 & 0 & 0 & 0 & 0 & 1 & 0 \\ v/L_0^2 & 1/L_0 & 0 & 0 & 0 & 0 & 0 & 0 & 1 \end{bmatrix}$$

where v, w, relative translation displacements of the nodes I and J expressed in the local axis system.

The equilibrium equation in the intermediate axis system is written as Eq. (17):

$$\{\Delta F_u\}=\left([B]^T[K_n][B]+[D]\right)\{\Delta S_u\} \tag{17}$$

The matrix $[D]$ is calculated by ignoring the displacement contribution due to u and the non-linear term due to vand the null matrix is denoted by 0. In the local axis system, by using transformation matrix $[T_0]$, the nodes' displacements in the local axis system are linked to the nodes' loads in the local axis system by eq. (18):

$$\{\Delta F_L\}=[T_0]^T\left([B]^T[K_n][B]+[D]\right)[T_0]\{\Delta S_L\} \tag{18}$$

where

$$[T_0]=\begin{bmatrix} -1 & 0 & 0 & 0 & 0 & 0 & 1 & 0 & 0 & 0 & 0 & 0 \\ 0 & -1 & 0 & 0 & 0 & 0 & 0 & 1 & 0 & 0 & 0 & 0 \\ 0 & 0 & -1 & 0 & 0 & 0 & 0 & 0 & 1 & 0 & 0 & 0 \\ 0 & 0 & 0 & 1 & 0 & 0 & 0 & 0 & 0 & 0 & 0 & 0 \\ 0 & 0 & 0 & 0 & 1 & 0 & 0 & 0 & 0 & 0 & 0 & 0 \\ 0 & 0 & 0 & 0 & 0 & 1 & 0 & 0 & 0 & 0 & 0 & 0 \\ 0 & 0 & 0 & 0 & 0 & 0 & 0 & 0 & 0 & 1 & 0 & 0 \\ 0 & 0 & 0 & 0 & 0 & 0 & 0 & 0 & 0 & 0 & 1 & 0 \\ 0 & 0 & 0 & 0 & 0 & 0 & 0 & 0 & 0 & 0 & 0 & 1 \end{bmatrix}$$

The element stiffness matrix in the local axis system can finally be written as Eq. (19):

$$[K_L]=[T_0]^T\left([B]^T[K_n][B]+[D]\right)[T_0] \tag{19}$$

Using the rotation matrix $[T_G]$, the equilibrium equation for the global axis system can be written as Eq. (20):

$$\{F_G\}=[T_G]^T[K_L][T_G]\{\Delta S_G\}=[K_G]\{\Delta S_G\} \tag{20}$$

The calculation organigram for the stage n of the beams loading is presented in Fig. 8.

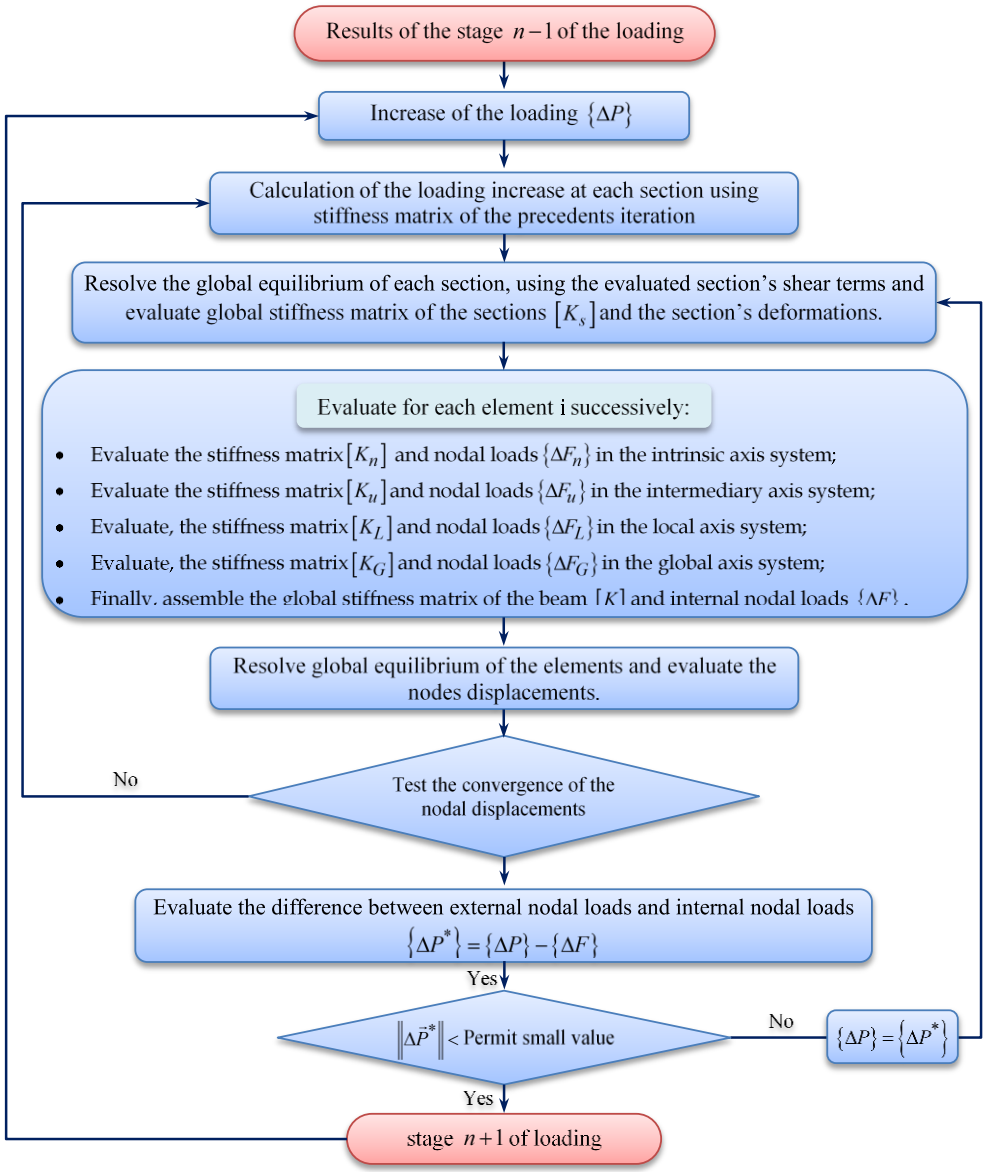

Fig. 8 – General organization of the calculation method

4 Reliability-model

The safety of a mechanical system is ensured by a safety coefficient: ratio between a loading variable and a resistance variable established by a deterministic approach. For a complex structure these efforts are poorly known, and its resistance is uncertain, so there is always a risk of seeing the structure ruined. For this purpose, the probabilistic approach allows to evaluate the risk by methods of reliability analysis of the mechanical systems developed during these last years. Because of many reasons (e.g. difficulty to express the material properties accurately, simplifications in the simulating of the behaviour of the structure, etc.), the 0% of failure probability cannot be guaranteed. However, the design can be performed to increase the reliability up to a selected level. In order to estimate the probability of failure of the examples studied in this paper, two methods are used, which are the level III method (direct Monte Carlo simulation) and the level II method (Hasofer-Lind).

4.1 Direct Monte Carlo simulation method

Monte Carlo simulations are the safest way to estimate the probability of failure. The integral to be assessed is:

$$P_f = \int_{Df} \phi_n(x_k)\, dx_1 dx_2 \cdots dx_n \tag{21}$$

where n is the number of simulation. By introducing a failure indicator I_{Df} :

$$I_{Df} = \begin{cases} 1 & si\ G(x_k) \le 0 \\ 0 & si\ G(x_k) > 0 \end{cases} \tag{22}$$

Integration of Eq. (21) can be given as:

$$P_f = \int_{R^n} I_{Df}\, \phi_n(x_k)\, dx_1 dx_2 \cdots dx_n = E\left[I_{Df} \right] \tag{23}$$

For n random draws, the empirical mean of I_{Df} is an estimate of P_f :

$$P_f = E\left[I_{Df} \right] \approx \frac{1}{n} \sum_{r=1}^{n} {I_{Df}}^r = \frac{N_f}{n} \tag{24}$$

The limit state function between the parameter space in a secure area and a failure area can be given as eq. (25):

$$G(\delta, P) = \delta_{\max} - \delta_{calcul} \tag{24}$$

where: $\begin{cases} G > 0 & \text{Defines the safe area} \\ G \le 0 & \text{Defines the failure area} \\ G = 0 & \text{Defines the limit state} \end{cases}$

4.1.1 Methodology

This consists of performing a large number of random draws k (that is, generating random variable realizations based on their joint probability density). The steps are as follows:

1- Estimate the value of the limit state function for each draw;

2- Examination of the function limit state for each draw;

→ *If* $G \le 0$ *There is failure, increment the counter of failed case based on the total number of performed attainments;*
→ *If* $G > 0$ *There is not failure, no incrementing the counter (failure indicator);*

3- Iterate the process from 1 to k until a sufficient number of draws is reached;

4- Evaluate the probability of failure by eq. (26):

$$P_f = \lim_{n \to \infty} \frac{\text{Number of events where } G \le 0}{\text{Total number of simulated events}} \tag{26}$$

The flowchart for calculating the probability of failure by direct Monte Carlo simulation is described below:

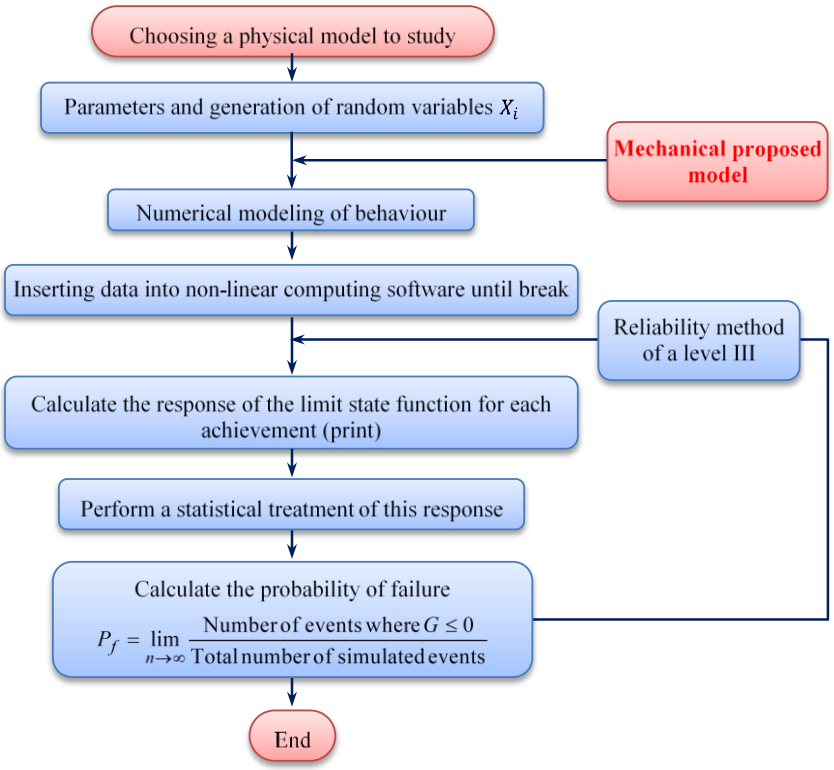

Fig. 9 – Flowchart for calculating the probability of failure by direct Monte Carlo simulation

4.2 Hasofer-Lind-Rackwitz-Fiessler (HL-RF) method [19, 22] :

The Hasofer-Lind-Rackwitz-Fiessler algorithm (HL-RF) is summarized by the following steps:

1- *Select a starting point* $\{u\}^{(0)}$;

2- *Evaluate the limit state function* $H\left(u^{(k)}\right)$;

3- *Evaluate the gradient of the limit state* $\{\nabla H(u)\}^{(k)}$ *and its norm* $\|\nabla H(u)\|^{(k)}$, *to deduce* $\{\alpha\}^{(k)}$ *by :*

$$\{\alpha\}^{(k)} = \frac{\nabla H\left(u^{(k)}\right)}{\|\nabla H(u)\|_{u^{(k)}}} ;$$

4- *Evaluate the reliability index* $\beta^{(k)}$;

5- *Evaluate the coordinate of the next iteration* $\{u\}^{(k+1)}$;

6- *Convergence test:*

if $\left\|\{u\}^{(k+1)} - \{u\}^{(k)}\right\| \le \varepsilon$; *stop the calculation ;*

else put $k = k+1$ *and go to the step 2.*

The organizational chart of Hasofer-Lind-Rackwitz-Fiessler (HL-RF) is described below:

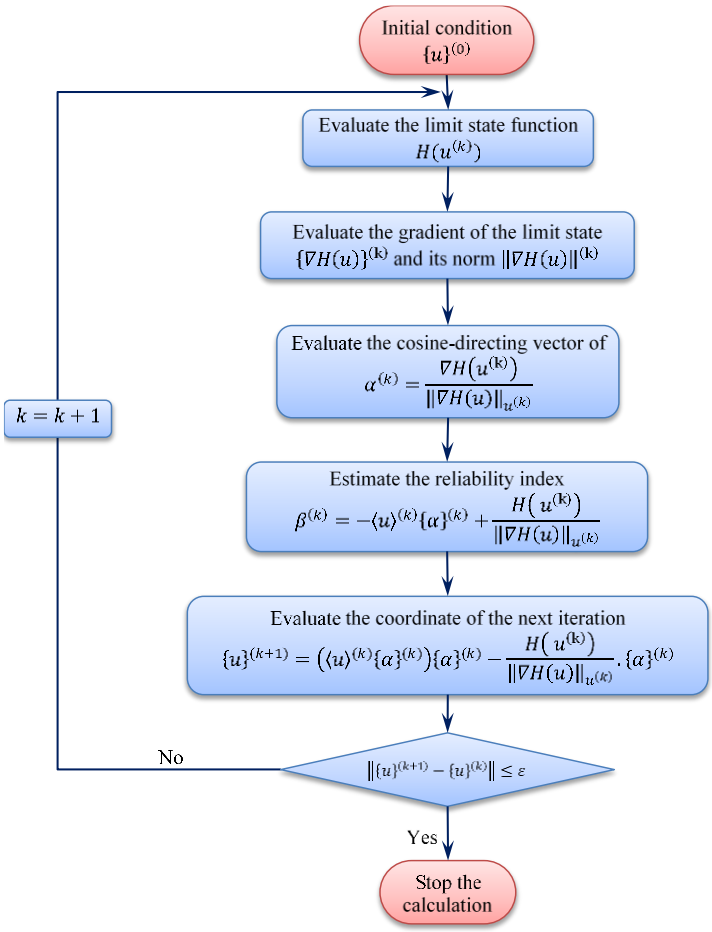

Fig. 10 – Organizational chart of Hasofer-Lind-Rackwitz-Fiessler (HL-RF)

The flow diagram of mechano-reliability coupling by analytical response surface is described below:

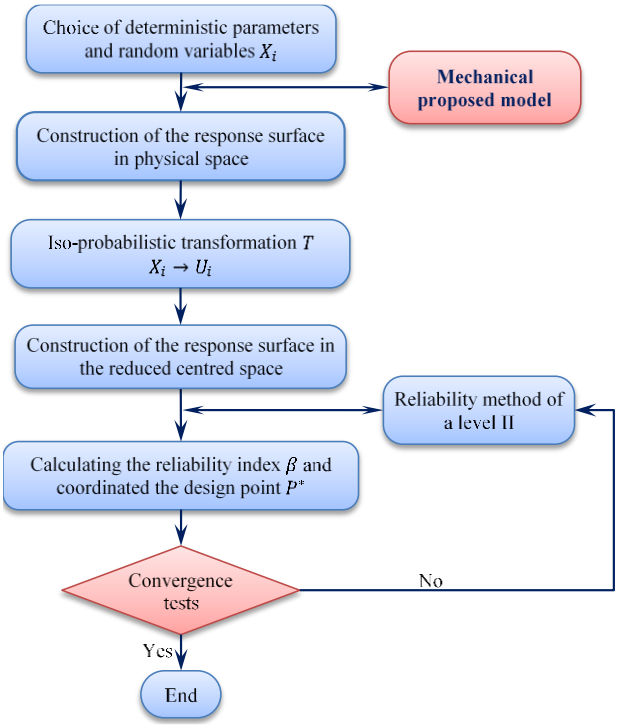

Fig. 11 – Organization chart of mechano-reliability coupling by surface of response

5 Numerical examples

5.1 Reinforced Concrete specimens with circular across section

To illustrate the reliability of the program developed in this present study. The calculation of three specimens with a circular cross section whose experimental study were carried out at Indonesia by Thamrinand al. [23] is presented.

Table 1 – Data reliabilities and mechanical characteristics of specimens

Variable	Unit	Probability law	Average	Standard deviation
$\boldsymbol{P}$	$[KN]$	Deterministic	Variable	–
Reinforcement	mm	Deterministic	BS-01 8Ø13	–
			BS-02 8Ø16	–
			BS-03 8Ø19	–
D	mm	Deterministic	250	–
$\boldsymbol{L}$	$[m]$	Deterministic	2.13	–
$\boldsymbol{v}$	–	Deterministic	0.2	–
$\boldsymbol{f_{cj}}$	$[MPA]$	Normal	20.1	2.01
$\boldsymbol{f_{tj}}$	$[MPA]$	Normal	1.806	0.180
$\boldsymbol{E_b}$	$[MPA]$	Normal	35656	3565.6
$\boldsymbol{\sigma_e}$	$[MPA]$	Normal	BS-01 394	39.4
			BS-02 380	38.0
			BS-03 400	40.0
$\boldsymbol{E_a}$	$[MPA]$	Normal	$2.05.10^5$	$2.05.10^3$
$\boldsymbol{k_b}$	–	Deterministic	2.15	–
$\boldsymbol{k'_b}$	–	Deterministic	1.15	–
$\boldsymbol{\varepsilon_{cu}}$	–	Normal	0.0035	0.00035
$\boldsymbol{\varepsilon_u}$	–	Normal	0.02	0.002

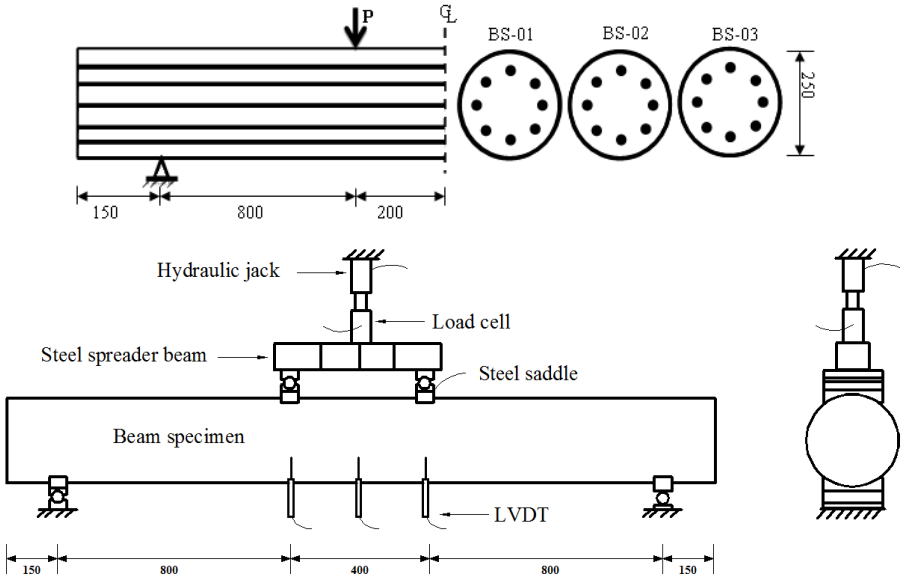

Fig. 12 – Schematic view of specimen's types, test arrangement, dimension, and equipment used Thamrin and al [23]

The diameters of longitudinal reinforcement were 13 *mm*, 16 *mm*, 19 *mm* with the yield strength of 394 *MPa*, 380 *MPa*, and 400 *MPa* respectively and the average concrete compressive strength obtained from compression tests was 20.1 *MPa*.

For all specimens (Fig.12), the clear span was 2000 *mm*; the distance between two-point loads was 400 *mm*, the shear span length was 800 *mm*, the end anchorage length beyond the support was 150 *mm*, and cross section diameter of 250 *mm*. The concrete covers were 30mm. More data related to the specimens is illustrated (in Table 1).

5.1.1 Evaluation of the deflection under load (P)

The simulation is projected to evaluate the vertical force (*P*) according to the vertical deflection in the middle of each specimen until they break. For this, we introduce the necessary data of specimens (see Table 1) in the computer program developed according to Fortran 90 standards. The evolution of the load as a function of displacement is shown in Figures (Figs.13-15).

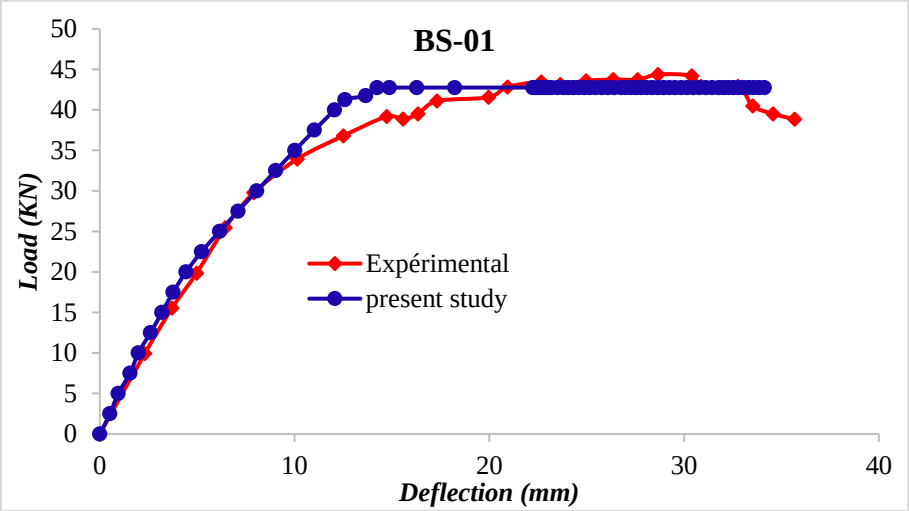

Fig. 13 – Evolution of the vertical deflection according to the load P for BS-01

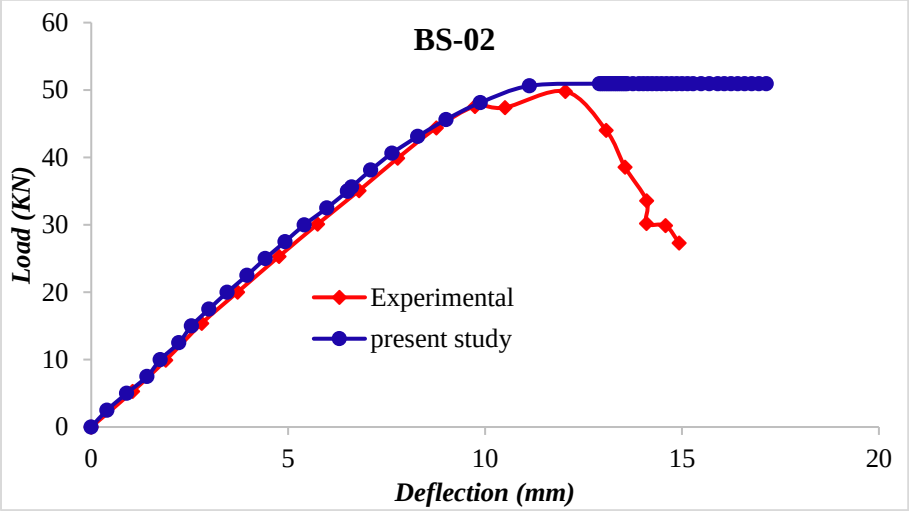

Fig. 14 – Evolution of the vertical deflection according to the load P for the BS-02

The curves, shown in Figures (Figs 13-15), approximate the experimental curves in phase of elastic behaviour, but at the onset of cracking phenomena, they begin to deviate from the experimental curves. This discrepancy is due to inaccuracies in the actual values for materials (such as the original elastic modulus of concrete or steel). Also, it can clearly be seen from the curves that our nonlinear calculation program shows a high capability to evaluates the resistance of the three-dimensional

structure elements with solid circular sections in reinforced concrete until the rupture in nonlinear elasticity under instant incremental loading.

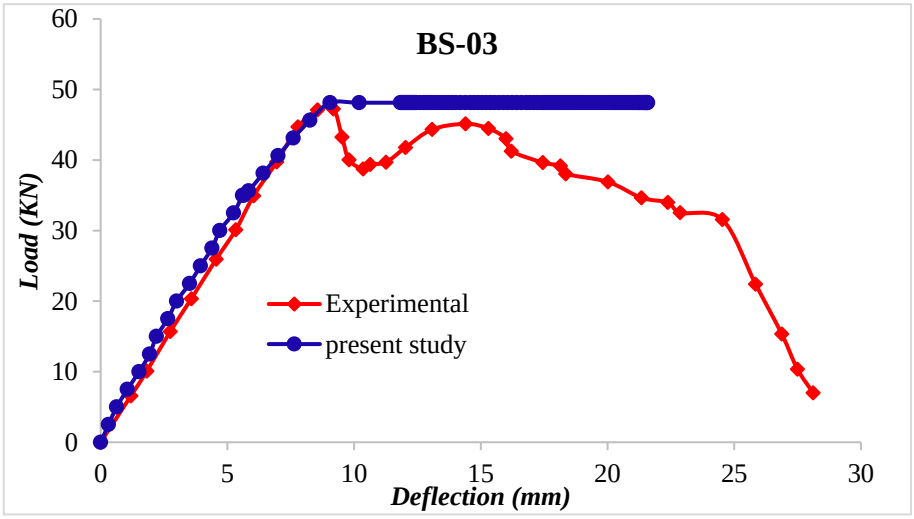

Fig. 15–Evolution of the vertical deflection according to the load P for BS-03

5.1.2 Evaluation of the failure probability of reinforced concrete specimens

In the next, we use two methods to estimate the probability of failure of the specimens: The Level II method (HL-RF) is used to calculate the probability of failure and the Level III method (Simulation Monte Carlo) to check the results of the Hasofer-Lind method.

a) By using the level II method (HL-RF)

It is kind of difficult to carry out the study by a direct coupling between a non-linear calculation program and a reliability program due to the complexity of finite element model, therefore it becomes necessary to build an analytical response surface.

Table 2 – Parameter laws of random variables for limit state of specimens

	BS-01		**BS-02**		**BS-03**	
X vector	X1	X2	X1	X2	X1	X2
Random variables	P	δ	P	δ	P	δ
Distribution law	Normal	Lognormal	Normal	Lognormal	Normal	Lognormal
Average μ	37.02576	0.02107	41.40104	0.01084	43.87500	0.01461
Standard deviation σ	11.66935	0.01057	15.36040	0.00518	10.91096	0.00595
Coefficient of variation ν	0.31516	0.50187	0.37101	0.47832	0.24868	0.40756

Table 3 – Results of mechanical reliability analysis of specimens obtained using (HL-RF) method

	BS-01	**BS-02**	**BS-03**
Reliability indexβ	1.5381	1.8813	1.7869
Probability of failure P_f	0.06301 (6.282%)	0.03065 (3.065%)	0.03754 (3.754%)
Reliability	0.93699 (93.699%)	0.96935 (96.935%)	0.96246 (96.246%)
Point centered design reduces space (U1, U2)	(0.35106, -1.09707)	(0.33221, -1.03816)	(0.84938, -2.65431)
Point of physical space design (X1, X2)	(30.4024, 0.0094)	(32.24, 0.00717)	(43.6185, 0.0068)

The random input variables are defined as parameters describing the non-linear behaviour of the material (concrete Young modulus, maximum compressive and tensile stress of the concrete, elastic limit of the reinforcement; reinforcement Young modulus) and their random distributions are given in Table 2. Other parameters, such as the length of the sample, are deterministic. After analysis by coupling mechanical reliability, the HL-RF method allowed us to obtain the results presented in Table 3.

b) By using Direct Monte Carlo simulation

After the Monte Carlo simulation analysis, we have the results presented in the Table 4:

Table 4 – Results of mechanical-reliability analysis of specimens obtained using direct Monte Carlo method

	BS-01	**BS-02**	**BS-03**
Probability of failureP_f	0.0405405 (4.05405%)	0.0675675 (6.75675%)	0.0135135 (1.35135%)
Reliability	0.9594595 (95.94595%)	0.9932433 (99.32433%)	0.9864865 (98.64865%)

It can be seen that the results obtained after Monte Carlo simulation analysis are close to those of the (HL-RF) method. These results lead to the need to deepen the knowledge of the properties of materials in order to improve the distribution parameters and take into account the correlations between random variables.

5.2 Reinforced concrete pile subject to composite bending

We carried out the calculation with the program on a pile whose experimental study was carried out at the CEBTP by Zhan [24], the pile studied in the context of this work has a diameter of 500 *mm* and 4 *m* long, under composite bending (see Fig.16).

Table 5 – Data reliabilities and Mechanicals characteristics of the pile

Variable	**Unit**	**Probability law**	**Average**	**Standard deviation**
P	[KN]	Deterministic	Variable	–
L	[m]	Deterministic	4.00	–
v	–	Deterministic	0.2	–
f_{cj}	[MPA]	Normal	42.41	4.241
f_{tj}	[MPA]	Normal	4.35	0.435
E_b	[MPA]	Deterministic	38059.47	–
σ_e	[MPA]	Normal	428	42.8
E_a	[MPA]	Normal	2.10^5	2.10^3
k_b	–	Deterministic	1.60	–
k'_b	–	Deterministic	0.60	–
ε_{b0}	–	Normal	0.0021	0.00021
ε_u	–	Normal	0.05	0.005

The normal compression force is 1370 *KN* (applied by means of external prestressing), the pile is reinforced longitudinally by 5 steel bars HA of diameter 16mm (corresponding to 0.5% by volume). The geometric characteristics and the detail of reinforcement is summarized in the following (Table 5).

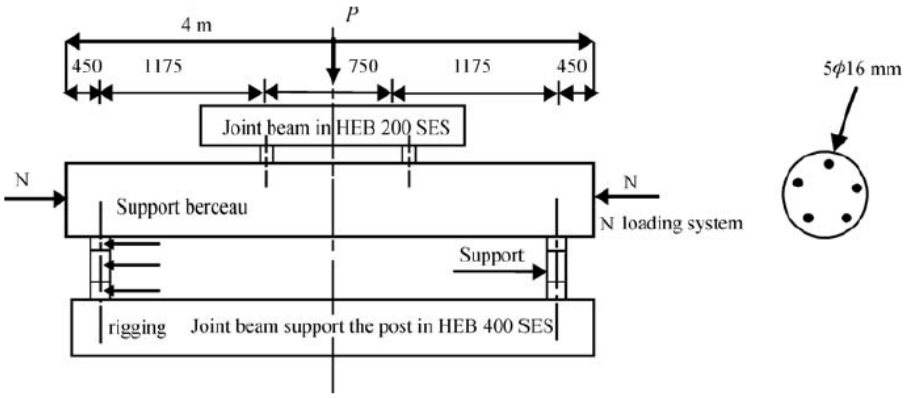

Fig. 16 – Composite bending test for reinforced concrete pile with circular cross section Zhan [24]

5.2.1 Evaluation of the deflection under load (P)

The aim of this simulation is to estimate the vertical Load (*P*) as a function of the vertical deflection at the middle of the pile until it breaks. For this, we introduce the necessary pile data (Table 5) into the computer program developed according to Fortran 90 standards. The behaviour laws used for numerical simulations are the Sargin law [3] for the behaviour of concrete in compression]and Grelat model for the concrete tensile behaviour Grelat [2]. As for the laws of behaviour of steels, we have taken those of elastoplastic. The evolution of the load as a function of the displacement is shown in figure (Fig. 17).

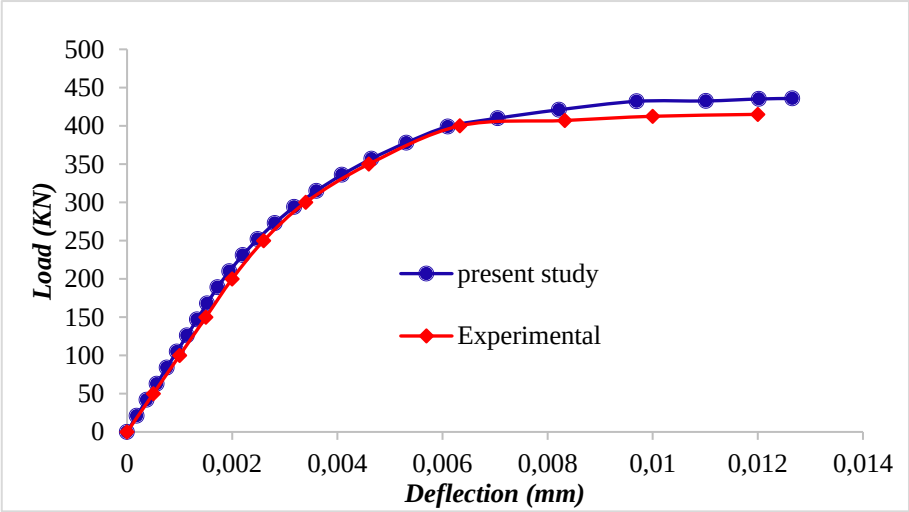

Fig.17 – Evolution of the vertical deflection according to the load P for the pile

It can clearly be seen in (Fig. 17) the good correlation between the curve obtained in this study and the experimental curve, the calculated maximum deflection is 0.01265 *m* for a real maximum deflection equal to 0.012 *m*, which means a difference of 1.05%.

5.2.2 Evaluation of the failure probability of the pile

a) By using The level II method (HL-RF)

The procedure for estimating random distributions of random variables (Figs. 18-19, Table 6) included in this study in order to bring the (real) statistical law closer to the structural reliability of the structures.

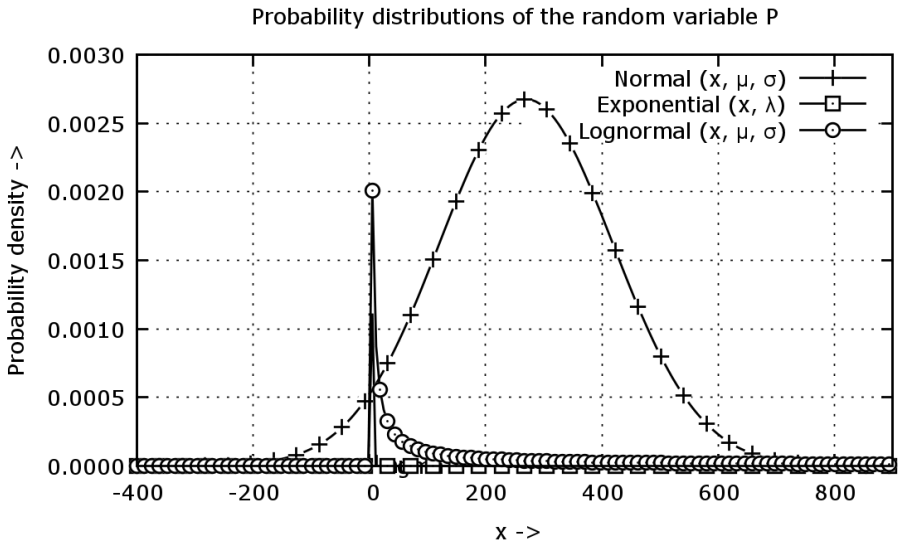

Fig. 18 –Probability distributions of the random variable P

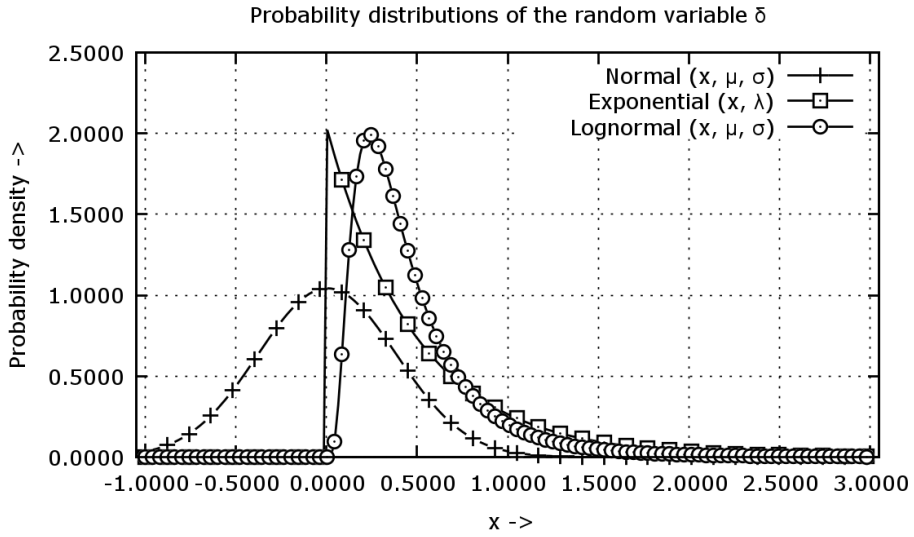

Fig. 19 – Probability distributions of the random variable δ

Table 6 – Parameter laws of random variables for limit state of the pile

X vector	**X1**	**X2**
Random variables	P	δ
Distribution law	Normal	Lognormal
Average μ	269.4581141	0.004223851
Standard deviation	149.1366442	0.003826062
Coefficient of variation ν	0.55346874	0.90582308

After analysis by coupling mechanical-reliability, the HL-RF method allowed us to obtain the results presented in Table 7.

The reliability index is $\beta = 1.6149$; which corresponds to a probability of failure of the pile estimated $P_f = \Phi(-\beta) = 5.282\%$, and resulting in a reliability of 94.715%. As for the most likely break point in physical space, it corresponds to load 221.378 *KN* and displacement to 0.0014 *m*.

Table 7 – Results of mechanical reliability analysis of the pile using (HL-RF) method

Reliability index	1.6149
Probability of failure	0.05282 (5.282%)
Reliability	0.94715 94.715%
Point centered design reduces space (U1, U2)	(0.4921, -1.5380)
Point of physical space design (X1, X2)	(221.378, 0.0014)

b) By using Direct Monte Carlo simulation method

By conducting the Monte Carlo simulation analysis, the obtained probability of failure is: $P_f = 3.3334\%$ so the structure (pile) is reliable at 96.6666%.These results represent a good agreement with those obtained by using the HL-RF method ($P_f = \Phi(-\beta)$ =5.282%).

In the next, another method is employed, where laws are combined with continuous random variables to get as close as possible to the real probability distributions of the random variables used in this example, for that we take only six cases of combination of the distribution laws. The six selected cases of random variables are presented in Table 8.

Table 8 – The different cases of the distributions' laws of the random variables

Random variables	Distribution law					
	Case 1	**Case 2**	**Case 3**	**Case 4**	**Case 5**	**Case 6**
P	Normal	Log-normal	Exponential	Exponential	Exponential	Normal
δ	Normal	Log-normal	Exponential	Log-normal	Normal	Log-normal

By using mechanical-reliability coupling of the six cases of combination between the laws of continuous random variables, the (HL-RF) method allowed us to obtain the following results:

Table 9 – Results of the mechano-reliability analysis for the different cases treated of the pile using (HL-RF) method

Case	Reliability index	Probability of failure	Design point (U1, U2)	Design point (X1, X2)	Reliability
Case 1	1.0958	0.1357 (13.57%)	(0.3339, -1.0437)	(180.937, 0.0018)	0.8643 (86.43%)
Case 2	0.6842	0.2483 (24.83%)	(0.2085, -0.0651)	(155.197, 0.0052)	0.7517 (75.17%)
Case 3	0.3285	0.3707 (37.07%)	(0.100, -0.3129)	(136.055, 0.0026)	0.6293 (62.93%)
Case 4	0.7216	0.2385 (23.85%)	(0.2199, -0.6872)	(157.362, 0.0022)	0.7615 (76.15%)
Case 5	0.6851	0.2451 (24.51%)	(0.2087, -0.6524)	(155.248, 0.0022)	0.7549 (75.49%)
Case 6	1.6149	0.05282 (5.282%)	(0.4921, -1.5380)	(221.378, 0.0014)	0.94715 (94.715%)

We noted for the different random variables that using the same distribution law (case 1, 2, 3), one obtains reliability indices smaller than nearly all reliability indices found using different distribution laws (case 4, 5, and 6). Consequently, a significant difference between the probability of failure of random variables with identical distribution laws (case 1, 2, and 3) and the failure probability of random variables with different distribution laws (case 4, 5, and 6) is observed.

In fact, all random variables may not follow the same law. We also find that case 6 gives the greatest reliability index $\beta = 1.6149$, hence a reliability of 94.715%, which confirms the accuracy of the first method used to estimate the laws of probability which allows to approximate the real statistical law of the random variable. In our study, we considered continuous and independent random variables, when in reality this is not the case for all systems.

6 Conclusion

The model presented in this study based on the stripe analysis of the circular cross sections using a variable shear modulus tanked into account not constant of the linear elasticity but variable with de shear strains variation. This model is able to predict the behaviour of the structure's elements, with circular cross sections, loaded in ending, axial load, and shear.

Circular sections equilibrium is solved using an iterative technique taking into account the real materials behaviour and variable shear modulus as a function of the shear strains variation.

The structure element's equilibrium is solved equally by a technique iterative based on the displacements method. The results obtained show that the model is able to predict global structures elements behaviour until a high value of the deflection. Indeed, the prediction results of the model compared with experimental results show that the model predictions are in good agreement with the experimental results in any field of the behaviour see Fig 17.

The application of the Response Surface Method has shown very high capability to estimate reliability index of nonlinear reinforced concrete structures with circular cross section. Monte Carlo method comes out to be the simplest method to implement, and the precision of the results depends mainly on the number of trials. The reliability model coupled with the mechanical model applied to the examples studied allowed us to evaluate the probability of failure relative to the ruin of mechanical systems with nonlinear behaviour. The choice of the nature of the random variables and their distribution remains the major problem; closely related to the user's concern and the scale of the study.

Notations

P : The applied load,

δ : Deflection,

L : The range,

h : The height,

v : Poisson ratio,

D : Cross section diameter,

f_{cj} : The compression characteristic strength,

f_{tj} : The tensile characteristic strength,

E_b : Concrete young modulus,

E_a : Steel young modulus,

σ : The stress,

σ_e : Yielding stress of the reinforcement,

k_b : Sargin law parameter,

k'_b : Sargin law parameter,

ε : The Strain,

ε_u : Ultimate strain of the reinforcement,

ε_{cu} : Ultimate concrete strain,

ε_{ct} : Concrete cracking strain,

ε_{rt} : Tensile concrete ultimate strain,

ε_0 : Concrete strain corresponding to f_{tj},

ε_e : Yielding strain of the reinforcement,

G : Shear modulus,

ns: number of bed passive reinforcements,

Aj: Section of the bare i ,

bi : Base width of the layer i ,

y_{ai}: Coordinate of the bare i ,

L_0 : Bar length before deformation,

L : Bar length after deformation,

M : Bending moment,

N : Normal load,

u, v : Longitudinal displacements of the nodes,

f_{et} : Yield stress of transverse reinforcement,

f_{el} : Yield stress of longitudinal reinforcement,

ρ_t : Is transverse reinforcement ratio,

ρ_l : Is longitudinal reinforcement ratio,

$[K_s]$: The section stiffness matrix in the intrinsic system,

$\{\Delta\delta\}$: is increase deformation vector of the section,

$\{\Delta F_s\}$: The vector of exterior loads increase,

$\Delta\varepsilon_g$: Cable element axial strain increase,

$\Delta\phi_y$: Curvature increase about *y*-axis,

$\Delta\phi_z$: Curvature increase about *z*-axis,

Δy_y : Shear deformation increase about *y*-axis,

Δy_z : Shear deformation increase about *z*-axis,

$\Delta\phi_x$: Torsional increase about *x*-axis,

ΔN : Axial load increase,

ΔM_y: Bending moment increase about y axis,

ΔM_Z : Bending moment increase about z axis,

ΔV_y : Shear increase in the y axis,

ΔV_Z : Shear increase in the z axis,

ΔM_c : Torsion moment increase,

$\{\Delta U\}$: Vector of nodes displacements increase,

$\{\Delta F\}$: Vector nodes forces increase,

$\{\Delta F_u\}$: Nodal loads increase in the intermediateaxis system,

$[B]$: Transformation matrix from intrinsic system to intermediateaxis system,

$\{\Delta S\}$: Vector of nodes displacements increase,

$\{\Delta S_u\}$: Nodal displacements in the intermediate axis system,

$[K_n]$: Element stiffness matrix in the intrinsicaxis system,

$\{\Delta F_n\}$: Nodal loads increase in the intrinsic axis system,

$\{\Delta S_n\}$: Nodal displacements in the intrinsicaxis system,

$\{\Delta F_L\}$: Nodal loads increase in the local axis system,

$\{\Delta S_L\}$: Nodal displacements in the localaxis system,

$[T_0]$: Translation matrix between intermediateaxis system and local axis system,

$\{\Delta F_G\}$: Nodal loads in the global axis system,

$\{\Delta S_G\}$: Nodal displacements in the global axis system,

$[T_G]$: Rotation matrix between local axis system to global axis system,

$[K_G]$: Stiffness matrix of the element in the global axis system,

$\{\Delta P\}$: Vector of applied loads increase,

$\{\Delta \varepsilon_n\}$: Normal strains increase,

$\{\Delta \varepsilon_t\}$: Shear strains increase,

$E_b(y,z)$: Concrete modulus,

$[D]$: Matrix of geometrical transformations,

G : Shear modulus,

I_{Df} : Indicator of failure

ϕ_n:The multi-normal density function

D_f : Failure domain

P_f : The probability of failure

β : Reliability index

$G(X1, X2)$: Function limit state

P^*: Point of the most probable failure,

m_R: Means strength,

m_s: Means loads,

σ_R: Standard deviations of the strength,

σ_s: Standard deviations of the loads,

$\alpha^{(k)}$: Vector cosine directors.

REFERENCES

[1]- S. Yaghmai, Incremental analysis of large deformations in mechanics of solids with applications to axisymmetric shells of revolution, Technical Report SESM 68–17, Univ. California, Berkeley. (1969).

[2]- A. Grelat. Nonlinear analysis of hyperstatic reinforced concrete frames. Thesis of Doctor Engineer. University Paris VI, French, 1978.

[3]- M. Sargin, Stress-Strain relationships for concrete and analysis of structural concrete sections. Study No. 4, Solid Mechanics Division, University of Waterloo, Waterloo, Ontario, Canada, (1971).

[4]- O. Nait-Rabah. Simulation numérique des ossatures spatiales. Thèse de doctorat, École Centrale de Paris, 1990.

[5]- F. Iguetoulene, Y. Bouafia, M.S. Kachi, Non linear modeling of three-dimensional reinforced and fiber concrete structures. Frontiers Struct. Civil Eng., 12(4) (2018) 439-453. doi:10.1007/s11709-017-0433-7.

[6]- F. Robert. Contribution à l'analyse non linéaire géométrique et matérielle des ossatures spatiales en Génie Civil : application aux ouvrages d'art. Thèse de doctorat Génie civil. INSA Lyon 1999.

[7]- C.A. Felippa, Nonlinear finite element methods. Aerospace Engineering Sciences Department of the University of Colorado. Boulder, 2001.

[8]- T. Rabczuk, J. Akkermann, J. Eibl, A numerical model for reinforced concrete structures. Int. J. Solid Struct., 42(5-6) (2005) 1327-1354. doi:10.1016/j.ijsolstr.2004.07.019.

[9]- G. Vasudevan, S. Kothandaraman, S. Azhagarsamy, Study on Non-Linear Flexural Behavior of Reinforced Concrete Beams Using ANSYS by Discrete Reinforcement Modeling. Strength Mater., 45(2) (2013) 231-241. doi:10.1007/s11223-013-9452-3.

[10]- M.S. Kachi, B. Fouré, Y. Bouafia, P. Muller, L'effort trenchant dans la modélisation du comportement jusqu' à rupture des pouters en béton armé et précontraint. Rev. Eur. Génie Civil, 10(10) (2006) 1235-1264. doi:10.1080/17747120.2006.9692914.

[11]- J.V. Frank, P.C. Michael, Predicting the Response of Reinforced Concrete Beams Subjected to Shear Using the Modified Compression Field Theory. ACI Struct. J., 85(3) (1988) 258-268. doi:10.14359/2515.

[12]- M. Kachi, Y. Bouafia, M. Saad, H. Dumontet, S. Bouhrat, Contribution to the calculation of reinforced concrete

circular sections by discrete reinforcement. Int. J. Eng. Technol., 6(1) (2014) 38-42. doi:10.7763/IJET.2014.V6.662.
[13]- E. Cosenza, C. Galasso, G. Maddaloni, A simplified method for flexural capacity assessment of circular RC cross-sections. Eng. Struct., 33(3) (2011) 942-946. doi:10.1016/j.engstruct.2010.12.015.
[14]- S.R.D. Gupta, K.S.M. Murty, Analysis/Design of Reinforced Concrete Circular Cross Sections. ACI Struct. J., 85(6) (1988) 617-623. doi:10.14359/2728.
[15]- D.M. Frangopol, Y. Ide, I. Iwaki. Effects of load path and load correlation on the reliability of concrete columns. In: Proceedings of the seventh specialty conference. Probabilistic Mechanics & Structural Reliability. Worcester. Massachusetts. USA: ASCE, 1996, pp. 206-209.
[16]- S.G. Reid. Strength and reliability of reinforced concrete columns with sustained loading. In: Proceedings of the seventh specialty conference. Probabilistic Mechanics & Structural Reliability. Worcester. Massachusetts. USA: ASCE, 1996, pp. 234-237.
[17]- M. Holicky, T. Vrouwenvelder. Time variant reliability of a reinforced concrete column. In: Advances in Safety and Reliability, ESREL'97 International Conference on Safety and Reliability, Lisbon, Pergamon, 1997, pp. 1307-1314.
[18]- D. Val, F. Bljuger, D. Yankelevsky, Reliability evaluation in nonlinear analysis of reinforced concrete structures. Struct. Saf., 19(2) (1997) 203-217. doi:10.1016/S0167-4730(96)00025-2.
[19]- K. Benyahi, Y. Bouafia, S. Barboura, M.S. Kachi, Nonlinear analysis and reliability of metallic truss structures. Frontiers Struct. Civil Eng. 12(4) (2018) 577-593. doi:10.1007/s11709-017-0458-y.
[20]- R.B. 91, modifiées 99 - Technical design rules and calculation of reinforced concrete structures and constructions, according to the method of limit states. Edition EYROLLES, French, 2000.
[21]- A. Adjrad, Y. Bouafia, M.S. Kachi, H. Dumontet, Non-Linear Modelling of Three Dimensional Structures Taking Into Account Shear Deformation. Int. J. Eng. Technol., 6(4) (2014) 290-298. doi:10.7763/IJET.2014.V6.715
[22]- M. Lemaire, Structural reliability. Editions Hermes Lavoisier ed. Paris, French: Wiley Online Library, 2005.
[23]- R. Thamrin, R. Kurniawan, A.P. Melinda, Shear and Flexural Capacity of Reinforced Concrete Members with Circular Cross Section. Proc. Eng., 171 (2017) 957-964. doi:10.1016/j.proeng.2017.01.400.
[24]- Z. Z. Contribution to the design ofpiles, reinforced concrete. Doctoral Thesis. University of Orleans, France, 1991.